Published in final edited form as:
Invest Radiol. 2013 June ; 48(6): 437–444. doi:10.1097/RLI.0b013e31828027c2.

Real-Time MRI-Guided Cryoablation of Small Renal Tumors at 1.5 T

Kamran Ahrar, MD[1,*], **Judy U. Ahrar, MD**[1], **Sanaz Javadi, MD**[1], **Li Pan, PhD**[2], **Denái R. Milton, MS**[3], **Christopher G. Wood, MD**[4], **Surena F. Matin, MD**[4], and **R. Jason Stafford, PhD**[5]

[1]Section of Interventional Radiology, The University of Texas MD Anderson Cancer Center, Houston, TX 77030

[2]Siemens Corporate Research and Technology, The University of Texas MD Anderson Cancer Center, Houston, TX 77030

[3]Department of Biostatistics, The University of Texas MD Anderson Cancer Center, Houston, TX 77030

[4]Department of Urology, The University of Texas MD Anderson Cancer Center, Houston, TX 77030

[5]Department of Imaging Physics, The University of Texas MD Anderson Cancer Center, Houston, TX 77030

Abstract

Objectives—Real-time magnetic resonance imaging (MRI)-guided cryoablation has been investigated in open MRI systems with low magnetic fields (0.2–0.5 T). More advanced imaging techniques and faster imaging rates are possible at higher magnetic fields which often require a closed-bore magnet design. However, there is very little experience with real-time interventions in closed-bore 1.5 T MRI units. Herein, we report our initial experience with real-time MRI-guided cryoablation of small renal tumors using a prototype balanced steady-state free precession (bSSFP) imaging sequence in a closed-bore 1.5-T MRI system.

Materials and Methods—From August 2008 to April 2012, 18 patients underwent MRI-guided cryoablation of small renal tumors. A 1.5-T cylindrical MRI scanner with a 125 cm × 70 cm bore and a prototype bSSFP sequence (BEAT IRTTT) were used to guide the placement of 17-gauge cryoprobes in real time. Ice ball formation was monitored every 3 minutes in one or more imaging planes. Each ablation consisted of 2 freeze-thaw cycles. Contrast-enhanced MRI was performed after the second active thaw period. Follow-up consisted of clinical evaluation and renal protocol computed tomography (CT) or MRI performed at 1, 6, 12, 18, and 24 months and annually thereafter.

Results—During the study period, we successfully ablated 18 tumors in 18 patients in 18 sessions. The mean tumor size was 2.2 cm (median, 2 cm; range: 1.2–4.4 cm). The number of cryoprobes used per patient was determined based on tumor size. The mean number of cryoprobes used per patient was 3 (median, 3 cryoprobes; range, 2–4 cryoprobes). Fifty-six cryoprobes, 9 biopsy needles, and 2 hydrodissection needles were successfully placed under real time MRI guidance using BEAT IRTTT sequence. Hydrodissection under MRI guidance was successfully performed in 4 patients. In each patient, contrast-enhanced MRI performed after the second active

[*]Corresponding author: Kamran Ahrar, 1515 Holcombe Boulevard, Unit 1471, Houston, TX 77030, Phone: 713-794-1097, Fax: 713-792-4098, kahrar@mdanderson.org.

LP is Staff Scientist at Siemens Corporate Research and Technology. For the remaining authors none were declared.

thaw period revealed a sharply defined avascular zone surrounding the targeted tumor, which confirmed complete ablation of the tumor with adequate margins. Although contrast media slowly accumulated in the targeted tumor in 9 patients immediately after the procedure, follow-up imaging studies performed at a mean of 16.7 months revealed no contrast enhancement within the ablation zone in these patients. Disease-specific, metastasis-free, and local recurrence–free survival rates were all 100%.

Conclusions—Real-time placement and manipulation of cryoprobes during MRI-guided cryoablation of small renal tumors in a closed-bore, high–magnetic field scanner is feasible. Technical and clinical success rates are similar to those of patients who undergo CT-guided radiofrequency ablation or cryoablation of small renal tumors. Our findings suggest that MRI-guided ablation has several advantages over CT-guided ablation, including real-time guidance for probe placement, multiplanar imaging, exquisite soft tissue contrast, and lack of ionizing radiation.

Keywords

Renal cell carcinoma; renal tumor; cryoablation; interventional MRI

Introduction

In selected patients who have small renal tumors and are not candidates for surgery, minimally invasive nephron-sparing therapy with radiofrequency ablation or cryoablation yields satisfactory oncologic outcomes.[1–4] Currently, most centers in the United States use computed tomography (CT) to guide the ablation of renal tumors. Despite its widespread use, CT is not an ideal imaging modality for guiding the ablation of renal tumors. For example, the density of renal tumors is often similar to that of normal renal parenchyma; therefore, non–contrast-enhanced CT images do not facilitate the detection of the tumor and determination of its boundaries (Fig. 1). In addition, conventional CT is limited to a single axial plane and is usually not performed in real time. Multidetector CT scanners can generate multiplanar reformatted images within seconds, but real-time CT-fluoroscopy is limited to a single axial plane. Furthermore, routine CT technique may expose patients to substantial amounts of ionizing radiation.[5]

In contrast to CT, magnetic resonance imaging (MRI) may have several advantages for guiding the ablation of renal tumors (Fig. 1). MRI provides exquisite soft-tissue contrast, which enables the detection of renal tumors and determination of their boundaries. Fast, real-time MRI in any arbitrary plane to facilitate accurate targeting of the tumor is feasible. In addition, real-time MRI monitoring of the ablation process can be performed without exposing the patient to ionizing radiation. Finally, MRI can be used to delineate the ablation zone to confirm the completeness of tumor ablation immediately after cryoablation has been performed.

Few studies have investigated the MRI-guided cryoablation of renal tumors,[6–10] and all of these studies were performed using open-configuration MRI systems with field strengths of only 0.2–0.5 T. More advanced MRI techniques and faster imaging rates are possible at higher magnetic fields (e.g. 1.5 T), which often requires a closed-bore magnet design. Yet, there are very few reports of real-time MRI guided interventions in closed-bore, high magnetic field MRI systems.[11,12] To our knowledge, there are no published reports of cryoablation for renal tumors in closed-bore, high field MRI system. The purpose of the present study was to investigate the feasibility and safety of real-time MRI-guided cryoablation of small renal tumors using a cylindrical bore 1.5-T MRI system using a prototype balanced steady-state free precession (bSSFP) imaging sequence (BEAT IRTTT).

Materials and Methods

Patients

The present study was approved by our institution's review board and complied with all Health Insurance Portability and Accountability Act regulations. We prospectively collected data for patients with renal tumors who underwent MRI-guided percutaneous cryoablation at our institution between August 2008 and April 2012. Patients' demographic data (age and gender) and clinical data (body mass index, side of kidney tumor, and tumor size) were recorded. Imaging and laboratory studies prior to, during, and after ablation were reviewed. Only those patients in whom real-time MRI guidance was used for placement of cryoprobes were included. All patients had been referred to our service by the urology department and were not candidates for surgery because of comorbidities.

Imaging Equipment

All procedures were conducted in an MRI suite dedicated to interventional procedures.[13] The suite is equipped with an 18-channel 1.5-T MRI scanner with a 125 cm X 70 cm cylindrical bore (MAGNETOM Espree, Siemens Medical System, Erlangen, Germany). The system has a maximum gradient amplitude of 33 mT/m and a slew rate of 170 T/m/s. Within the suite, the radiologist performing the procedure can view images on 2 portable consoles equipped with radiofrequency-shielded monitors and use 3 interfaces to control table movement and initiate or stop scanning. An MRI-compatible fiber optic communication system (IMROC, OptoAcoustics, Ltd., Or-Yehuda, Israel) provides the radiologist with hearing protection and enables the radiologist to communicate with the MRI technologist in the control room and the anesthesiologist performing breath holds during needle placement. For signal reception, standard diagnostic phased array coils were used. These included a spine array insert and a 6-channel body matrix array, which has four 10 cm × 10 cm openings positioned directly over the probe insertion site.

Technique

Because of their speed, high signal-to-noise ratio, and T2-like contrast, balanced steady-state free precession (bSSFP) acquisitions were used as the primary imaging techniques for planning and targeting.[14] In situations where little contrast is afforded owing to similar T1 values in tissue, bSSFP offers contrast based on the differences in T2 based on its T2/T1 weighting at larger flip angles. Initial imaging of the target tumor included a 3-plane bSSFP localizer followed by a higher resolution bSSFP acquisition, in one of the conventional imaging planes (e.g., axial, sagittal, or coronal). Because the scanner's closed bore and the small opening in the surface coil limited the radiologist's access to the patient, puncture sites were marked with the patient positioned outside the bore of the magnet in a fashion similar to that used in CT-guided interventions. With the patient outside the bore of the scanner, the radiologist inserted the cryoprobe into the subcutaneous soft tissues at an angle determined using planning images. The patient was then moved to the isocenter of the magnet, and continuous real-time imaging of the kidney was initiated. The radiologist then reached into the bore of the magnet and advanced the probe to the desired location within the tumor.

Real-time imaging utilized a prototype interactive bSSFP pulse sequence (BEAT IRTTT; Siemens Corporate Research; sequence author, Li Pan). BEAT is the production cardiac sequence which was modified in this prototype for interactive real-time tip tracking (IRTTT). The acquisition parameters varied according to the weight of the patient, field of view, and scan plane orientation but were generally similar (TR, <4 ms; TE, < 3 ms; flip angle, 50°–70°; acquisition matrix, 192 × 192, receiver bandwidth, > 500 Hz/pixel). This facilitated acquisition times of < 1 second per slice for 3 parallel, sequentially acquired planes 4-mm in thickness with a 1-mm gap. The prototype software displayed these planes

in a montage on the MR console as well as a cross-table monitor in the MRI suite for the radiologist. All real-time guidance was performed during anesthesiologist-directed patient breath holds. The interactive nature of the acquisition enabled the technologist to adjust the scan plane orientation and location at the command of the radiologist without having to stop imaging. Planning of the ablation, probe placement verification, and monitoring were performed using a standard implementation of bSSFP on the scanner (TR, < 4 ms; TE, < 2 ms; flip angle, 50°–70°; receiver bandwidth, >500 Hz/pixel; acquisition matrix, 256 × 192 for 24-cm to 36-cm fields of view) and a slice thickness of 5 mm with no gap for up to 20 slices in less than 20 seconds acquired during a breath hold. When appropriate, chemically selective fat saturation was used to improve the visualization of the tumor or cryoprobes. Because magnetic susceptibility-induced signal losses degraded the quality of the bSSFP acquisition after the placement of 2 or more cryoprobes, a multi-slice HASTE sequence (TR, 2000 ms; TE, 83 ms; refocusing pulse, 150°; matrix, 192 × 192 with 60% partial Fourier encoding coverage; receiver bandwidth, 500 Hz/pixel) was used to verify the position of the cryoprobes (Fig.2). Occasionally, a breatthold T1-W fast spin echo (TR, 400 ms; TE, 4.4 ms; slice thickness, 4mm; gap,1mm; echo-train length, 7; rBW=789Hz/pixel; matrix, 192×144; acquisition time, 5–10 interleaved planes in 8–12 seconds) was used to reduce metal artifacts. The field of view and TR varied to accommodate interleaved slices and alleviate specific absorption ratio (SAR) limits.

For ice ball monitoring, multiplanar images using either the bSSFP or half Fourier acquired single shot turbo spin echo (HASTE) sequence were collected every 3 minutes and reformatted so the radiologist could assess the ice ball relative to the surrounding anatomy. In addition to standard axial, sagittal, or coronal planes, images were reformatted parallel and/or perpendicular to the plane of individual cryoprobes to better delineate the relationship of the ice ball with the adjacent anatomy. After the ablation procedure, a multi-phase contrast-enhanced 3-dimensional radiofrequency spoiled gradient-recalled echo volume interpolated breath hold examination (VIBE) acquisition with fat saturation was used to verify the region of perfusion deficit predicted by the position of the ice ball on the monitoring slices. Specific parameters for various acquisitions are presented in Table 1.

Anesthesia and Patient Monitoring

An MRI-compatible ventilator (Narkomed MRI-2, Dräger Medical AG, Lubeck, Germany) is available in the iMRI suite at all times. All patients were under general anesthesia at the time of cryoablation. MRI-compatible hemodynamic monitoring equipment (Precess 3160; Invivo, Orlando, FL) was used to monitor patients according to the standard of care for patients under general anesthesia.

Biopsy Equipment and Technique

For MRI-guided renal tumor biopsy, we used a coaxial system consisting of MRI-compatible 16 gauge guide needle and 18 gauge semiautomatic core biopsy needle (Invivo Corporation). The semiautomatic core biopsy needles have an adjustable length allowing acquisition of 10 or 20-mm long core biopsy samples. At least two core biopsy samples were obtained from each tumor.

Cryoablation Equipment and Treatment Delivery

For cryoablation, we used an MRI-compatible cryoablation system (MRI Seednet Cryoablation System; Galil Medical, Yokeneam, Israel) that comprised a computer workstation housed in the MRI control room, a gas distribution apparatus, and disposable cryoprobes. The system delivers argon and helium (the tanks of which are also housed in the MRI control room) through a junction box to an MRI-compatible gas distribution unit. Several (up to 25) MRI-compatible cryoprobes can be attached to the gas distribution unit

during cryoablation procedure. Two types of MRI-compatible cryoprobes, IceRod and IceSeed (both from Galil), were used in the study. Both probes are 1.47 mm in diameter (17 gauge) and 17.5 cm long. To facilitate their use within the bore of the MRI system, the probes' handles are at right angles to their shafts. The IceRod creates an oval to teardrop-shaped ice ball, whereas the IceSeed creates a smaller, more spherical ice ball.

Depending on the size of the tumor[15], 1–4 cryoprobes were used to perform two freeze-thaw cycles lasting 10–15 minutes each. Treatment was considered technically successful if MRI safely provided planning, targeting, monitoring and post-treatment verification of the target tumor in a single session. Patients were admitted to an outpatient unit for overnight observation.

Patient Follow-up—Follow-up consisted of clinical evaluation and renal protocol CT or MRI at 1, 6, 12, 18, and 24 months, and once a year thereafter.[16]

Statistical Analysis

Percentages and frequencies were used to summarize categorical measures and means, standard deviations, medians, and ranges were used to summarize continuous measures. Overall survival was computed from the date of cryoablation to the last follow-up or death. Patients alive at the last follow-up date were censored with regard to overall survival. Similarly, cancer-specific survival was computed from the date of the MRI-guided cryoablation to last known vital status. Patients who died of causes other than cancer were censored at the date of their deaths, whereas patients who were alive at the last follow-up date were censored at that time. Lastly, time-to-local recurrence of disease was computed from the date of the MRI-guided cryoablation to the date of the last available imaging study, when recurrence was assessed. Kaplan-Meier survival curves were used to estimate overall and cancer-specific survival rates. All statistical analyses were performed using SAS 9.3 for Windows (SAS Institute Inc., Cary, NC).

Results

During the study period, 18 patients with 18 renal tumors underwent real-time, MRI-guided cryoablation in 18 sessions. Patient demographics are given in Table 2. The mean tumor diameter was 2.2 cm (median, 2 cm; range, 1.2–4.4 cm). The body mass index for the patients ranged from 20.7 to 42.7 (mean, 28.9±5.6).

Core biopsy samples of tumors were obtained from 9 patients immediately before the cryoablation procedure. All 9 biopsies were performed under real-time MRI guidance. Another 6 patients underwent renal biopsy at an earlier visit. Of those patients, 3 underwent CT guided biopsy and 3 others had MRI guided biopsy. Histopathologic evaluation revealed renal cell carcinoma in all 15 of these patients. Biopsy was not performed in 3 patients; of these patients, 2 had histopathologically confirmed renal cell carcinoma in the same or contralateral kidney, and 1 had history of Von Hippel-Lindau disease and biopsy-proven renal cell carcinoma.

All treatments were considered technically successful. The mean number of cryoprobes used to ablate each tumor was 3 (range, 2–4). Real-time MRI guidance was used to place 56 cryoprobes in 18 patients. Real-time guidance was also used to place 9 biopsy needles and 2 needles for hydrodissection. In 8 cases, a combination of sagittal, axial, sagittal-oblique, and axial-oblique imaging planes were used to guide placement of cryoprobes and needles. In 10 cases, only an axial plane was used. In two patients, after placement of 3 or more probes, modified sequences were used to reduce the magnetic susceptibility artifact from the probes. These sequences were optimized by maximizing the bandwidth, generally resulting in higher

specific absorption rates (SAR). Immediately after initiation of imaging with these pulse sequences, the interventional radiologist noticed involuntary jerking motion of the patient and the probes. In both cases, the imaging was stopped immediately, wires and connections were checked, and parameters were modified to lower the SAR. Repeat imaging was successful without any further nerve stimulation. Both procedures were successfully completed.

MRI-guided hydrodissection used to separate loops of bowel adjacent to the intended ablation zone was successfully accomplished under MRI guidance in 4 patients (Fig.3). Freeze rates and times for each probe were modulated based on MRI feedback of the ice ball until the visualized ice ball extended well beyond the boundaries of the targeted tumor. MRI provided consistent contrast of the ice ball edges in all tissue environments, including fatty tissue. Dynamic contrast-enhanced MRI performed after tumor ablation revealed perfusion deficits within the expected area of damage based on correlation with the location of ice ball visualization (Fig. 1). In all patients, the ablation zone completely encompassed the targeted tumor. In 9 patients, MRI revealed slow accumulation of contrast media within the targeted tumor. However, follow-up imaging studies revealed no contrast in all targeted tumors.

All patients were discharged from the hospital fewer than 24 hours after undergoing tumor ablation. There were no major complications, 4 patients experienced minor complications. Two patients had postprocedural pain; 1 patient complained of paresthesias and numbness in a bandlike distribution in the abdominal wall; and 1 patient with a central tumor had small perinephric hematoma and gross hematuria immediately after the procedure. The last patient's hematuria resolved before the patient was discharged from the hospital.

The mean time between cryoablation and last follow-up was 16.4 months (median, 11 months; range, 1–39 months). Sixteen patients (89%) were alive at last follow-up. Two patients died of causes unrelated to the renal tumor or the procedure. One patient developed a new tumor at a different site within the same kidney. No patients developed distant metastases. The rates of overall, disease-specific, and metastasis-free survival were 88.9%, 100%, and 100%, respectively (Figs. 4 and 5).

Discussion

In the present study, we demonstrated the safety and feasibility of using a prototype, real-time imaging sequence in a closed-bore, 1.5T MRI scanner to perform MRI-guided cryoablation of small renal tumors.

According to guidelines established by the American Urological Association in 2009, the treatment of choice for small renal tumors is partial nephrectomy.[17] However, thermal ablative therapies including cryoablation are acceptable alternatives for carefully selected patients.[17] In general, good candidates for percutaneous image-guided tumor ablation include patients who may not be suitable for surgery because of medical comorbidities and patients with one kidney, chronic kidney disease, prior partial nephrectomy, or multifocal small renal tumors.[18] Excellent outcomes after percutaneous cryoablation of small renal tumors have been reported.[4] Most published series report the procedure being performed primarily under CT guidance supplemented with or without ultrasonography. Few small series have reported on MRI-guided cryoablation of renal tumors.[6–10] In 2001, Shingleton and Sewell reported using T1-weighted fast spin echo (FSE) images from an open-configuration 0.5-T MRI system (Signa SP 0.5T; GE Medical Systems; Milwaukee, WI) to guide cryoprobe placement and monitor ice ball formation and thawing in 20 patients with 22 tumors.[6] In their study, they placed the cryoprobes using a Seldinger technique through an introducer sheath. At a mean follow up of 9 months, there were no recurrent tumors. In

2005, Silverman et al. reported their experience with a 0.5-T MRI system, which was identical to that used by Shingleton and Sewell, to ablate 26 tumors in 23 patients.[6] In that study, all patients were treated while under general anesthesia. Cryoprobes were placed in tandem alongside an MRI-compatible 22–20 gauge biopsy needle, and gradient recalled echo images or T2- or T1-weighted FSE images were used to monitor ice ball formation and thawing every 1–3 minutes. The mean number of cryoprobes used per patient was 2.4 (range, 1–4 cryoprobes). Acquisition times ranged from 20 to 60 seconds. Technical success was achieved 24 of 26 tumors (92%). Follow-up MRI revealed residual or recurrent tumors in 3 patients (13%), resulting in a recurrence-free survival rate of 87%.

Unlike previous studies, in which low-field, open-configuration MRI systems were used to guide cryoablation, we used a high-field (1.5-T) cylindrical bore MRI system to guide cryoablation. In the present study, the initial technical success and local recurrence-free survival rates were both 100%. We easily identified all tumors using fast T2-like imaging sequences (i.e., bSSFP) with acquisition times of <1 second per acquired plane. Real-time MRI guidance facilitated the placement of 56 cryoprobes in 18 patients who remained within the bore of the scanner and the placement of biopsy needles prior to cryoprobe placement in 9 patients. In 8 complex cases, a combination of sagittal, axial and oblique imaging planes was used to accurately image and advance each cryoprobe in real-time. Additional MRI guidance also facilitated the placement of needles for hydrodissection to minimize the risk of bowel injury in 4 patients. The installation of normal saline into the perinephric space was easily visualized in real-time using bSSFP or HASTE imaging sequences. The multiplanar imaging capability of MRI facilitates the accurate determination of the distribution of fluid injected during hydrodissection (Fig. 3). We performed dynamic contrast-enhanced MRI to evaluate the perfusion deficit within the expected ablation zone. Non-contrast forms of assessing cryoablation damage are important, particularly in patients with severe chronic kidney disease. In the future, techniques such as arterial spin labeling, BOLD imaging and diffusion-weighted intravoxel incoherent motion imaging, may provide this function.[19] However, these techniques would need to be validated independently for post-therapy treatment validation as often residual ice, or cold spots in the treatment zone, may produce confounding results.

Despite numerous advantages, the current state of technology poses a few challenges in using MRI guidance for ablation of renal tumors. The process of selecting and marking probe-insertion sites using the current system is still cumbersome and time-consuming. It requires expertise by technologist and physician routinely performing MRI guided procedures. Unlike CT, MRI guided interventions require placement of surface coils on the patient. In the present study, we placed a standard Siemens body matrix array coil on the backs of the patients, who were placed in a prone position on the MRI table containing a spine matrix array. The 10×10 cm opening in the body matrix array limits access to the probe insertion site. Multiple cryoprobes must be inserted close to one another which may cause exaggerated susceptibility. Similarly, insertion of additional cryoprobes, biopsy, or hydrodissection needles is limited to a very small access site. Having access to a larger surface area gives the radiologist more flexibility in selecting insertion sites for various needles and probes and may reduce the susceptibility artifact from those devices. This is an important issue and can be easily remedied with development of surface coils designed specifically for MRI-guided interventions.

Using bSSFP imaging sequences results in the MRI-compatible cryoprobes having relatively small magnetic susceptibility artifacts on MR images. Thus, the placement of the first and second cryoprobes is relatively easy because the probes' magnetic susceptibility artifacts do not overlap, which enables the visualization of the probes as well as the targeted tumor. However, the placement of additional probes becomes increasingly difficult as the probes'

magnetic susceptibility artifacts merge. In cases in which the operator had difficulty using bSSFP sequences to identify and locate the tips of the third and fourth cryoprobes, we used a 3-dimensional T1-weighted FSE or HASTE imaging sequence to minimize the blooming artifacts and visualize the entire length of the individual probes. We expect that in the future, as cryotechnology is refined and more effective cryoprobes are developed, one can create larger ice balls using fewer cryoprobes.

Although bSSFP sequences for planning cryoablation were fast and provided excellent soft-tissue contrast, they did not facilitate the visualization of small ribs. When selecting a needle path to a renal tumor, occasionally we had difficulty identifying the overlying ribs with confidence. Previous experience has taught us that when we mark a planned probe insertion site on a patient, we should also mark the axial or sagittal imaging plane, which enables us to move the inserted probe within the imaging plane. Of course, this strategy is limited by the small opening in the surface coil through which we access the patient.

Another limitation of our system was real-time image display. In the present study, all patients were placed in the prone position. During real-time or intermittent imaging for targeting, the prototype software displays the images in the default radiological coordinate system (i.e., the ventral body surface appears at the top of the image and the dorsal surface of the patient appears at the bottom). During needle guidance, the discrepancy between the position of the patient on the table and the image on the in-room monitor can disorient the physician placing the needle. In addition, in patients in whom multiple probes have been placed, we noted occasional nerve stimulation during imaging using sequences such as fat suppressed bSSFP or HASTE. These sequences, which resulted in higher SAR than typical real-time or intermittent imaging sequences did, were usually incorporated when susceptibility artifacts from multiple probes made verification of probe placement difficult. Stimulation always ceased when the acquisition SAR was reduced and was usually accomplished by forgoing fat suppression, reducing the flip angle, or slowing the sequence down.

Finally, the real-time imaging sequence (BEAT IRTTT) that was used in this study is a prototype developed by Siemens Corporate Research and is not commercially available as of the time of this writing. The sequence is fully compatible with the current software platform for Siemens MRI scanners and does not require any additional software or hardware. We anticipate that once released, it would be easy to adopt by individual practices.

In summary, we have demonstrated the feasibility and safety of using a prototype, real-time imaging sequence in a closed-bore, high magnetic field MRI unit to guide cryoablation of small renal tumors. It was a small study with relatively short follow-up. Larger studies are needed to determine any possible limitations of the MRI system compared to CT for treatment of tumors in different locations within the kidneys. Longer follow-up is also needed to confirm oncologic efficacy of the cryoablation system used in the MRI suite. Additional work is needed to further refine the imaging sequences, enhance the ability of the operator to change plane of imaging in real time, and to change display of images in real time as needed for each case. Development of surface coils designed for interventional procedures and more effective cryoablation systems can help advance this technology in the future.

Acknowledgments

Source of Funding: This research was supported in part by the National Institutes of Health through MD Anderson’s Cancer Center Support Grant CA016672

REFERENCES

1. Zagoria RJ, Pettus JA, Rogers M, Werle DM, Childs D, Leyendecker JR. Long-term outcomes after percutaneous radiofrequency ablation for renal cell carcinoma. Urology. 2011; 77:1393–1397. [PubMed: 21492910]
2. Tracy CR, Raman JD, Donnally C, Trimmer CK, Cadeddu JA. Durable oncologic outcomes after radiofrequency ablation: experience from treating 243 small renal masses over 7.5 years. Cancer. 116:3135–3142. [PubMed: 20564644]
3. Levinson AW, Su LM, Agarwal D, et al. Long-term oncological and overall outcomes of percutaneous radio frequency ablation in high risk surgical patients with a solitary small renal mass. J Urol. 2008; 180:499–504. discussion. [PubMed: 18550123]
4. Atwell TD, Callstrom MR, Farrell MA, et al. Percutaneous renal cryoablation: local control at mean 26 months of followup. J Urol. 2010; 184:1291–1295. [PubMed: 20719341]
5. Leng S, Atwell TD, Yu L, et al. Radiation dose reduction for CT-guided renal tumor cryoablation. AJR Am J Roentgenol. 2011; 196:W586–W591. [PubMed: 21512049]
6. Shingleton WB, Sewell PE Jr. Percutaneous renal tumor cryoablation with magnetic resonance imaging guidance. J Urol. 2001; 165:773–776. [PubMed: 11176465]
7. Silverman SG, Tuncali K, vanSonnenberg E, et al. Renal tumors: MR imaging-guided percutaneous cryotherapy--initial experience in 23 patients. Radiology. 2005; 236:716–724. [PubMed: 16040927]
8. Miki K, Shimomura T, Yamada H, et al. Percutaneous cryoablation of renal cell carcinoma guided by horizontal open magnetic resonance imaging. Int J Urol. 2006; 13:880–884. [PubMed: 16882047]
9. Kodama Y, Abo D, Sakuhara Y, et al. MR-guided percutaneous cryoablation for bilateral multiple renal cell carcinomas. Radiat Med. 2005; 23:303–307. [PubMed: 16012408]
10. Harada J, Dohi M, Mogami T, et al. Initial experience of percutaneous renal cryosurgery under the guidance of a horizontal open MRI system. Radiat Med. 2001; 19:291–296. [PubMed: 11837579]
11. Stattaus J, Maderwald S, Forsting M, Barkhausen J, Ladd ME. MR-guided core biopsy with MR fluoroscopy using a short, wide-bore 1.5-Tesla scanner: feasibility and initial results. J Magn Reson Imaging. 2008; 27:1181–1187. [PubMed: 18425833]
12. Woodrum DA, Mynderse LA, Gorny KR, Amrami KK, McNichols RJ, Callstrom MR. 3.0T MR-guided laser ablation of a prostate cancer recurrence in the postsurgical prostate bed. J Vasc Interv Radiol. 2011; 22:929–934. [PubMed: 21708319]
13. Ahrar K, Stafford RJ. Magnetic resonance imaging-guided laser ablation of bone tumors. Tech Vasc Interv Radiol. 2011; 14:177–182. [PubMed: 21767785]
14. Scheffler K, Lehnhardt S. Principles and applications of balanced SSFP techniques. Eur Radiol. 2003; 13:2409–2418. [PubMed: 12928954]
15. Littrup PJ, Jallad B, Vorugu V, et al. Lethal isotherms of cryoablation in a phantom study: effects of heat load, probe size, and number. J Vasc Interv Radiol. 2009; 20:1343–1351. [PubMed: 19695903]
16. Matin SF, Ahrar K, Cadeddu JA, et al. Residual and recurrent disease following renal energy ablative therapy: a multi-institutional study. J Urol. 2006; 176:1973–1977. [PubMed: 17070224]
17. Novick AC. Guideline for managment of the clinical stage 1 renal mass. http://wwwauanetorg/content/media/renalmass09pdf.
18. Ahrar K, Wallace MJ, Matin SF. Percutaneous radiofrequency ablation: minimally invasive therapy for renal tumors. Expert Rev Anticancer Ther. 2006; 6:1735–1744. [PubMed: 17181487]
19. Chandarana H, Kang SK, Wong S, et al. Diffusion-Weighted Intravoxel Incoherent Motion Imaging of Renal Tumors With Histopathologic Correlation. Invest Radiol. 2012

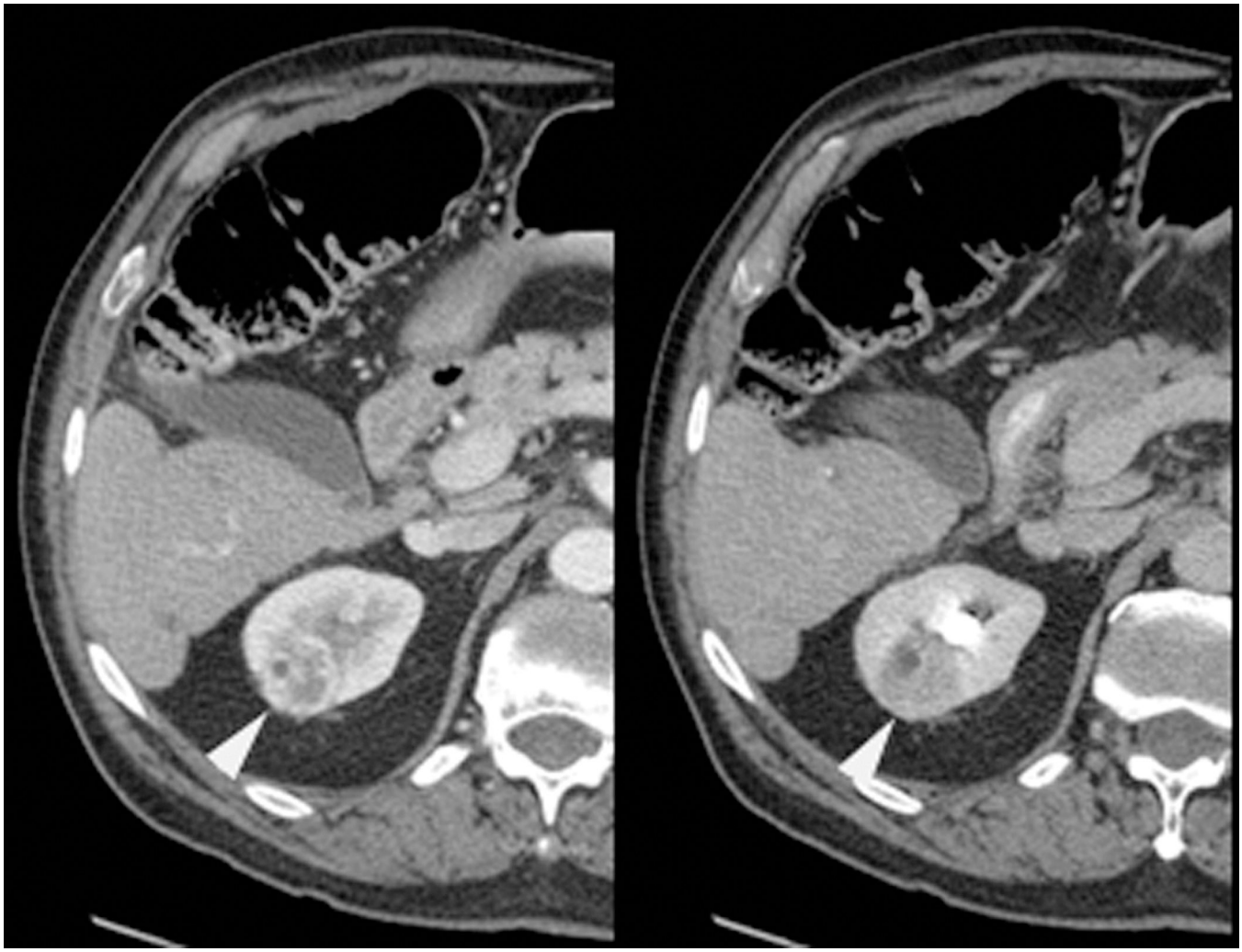

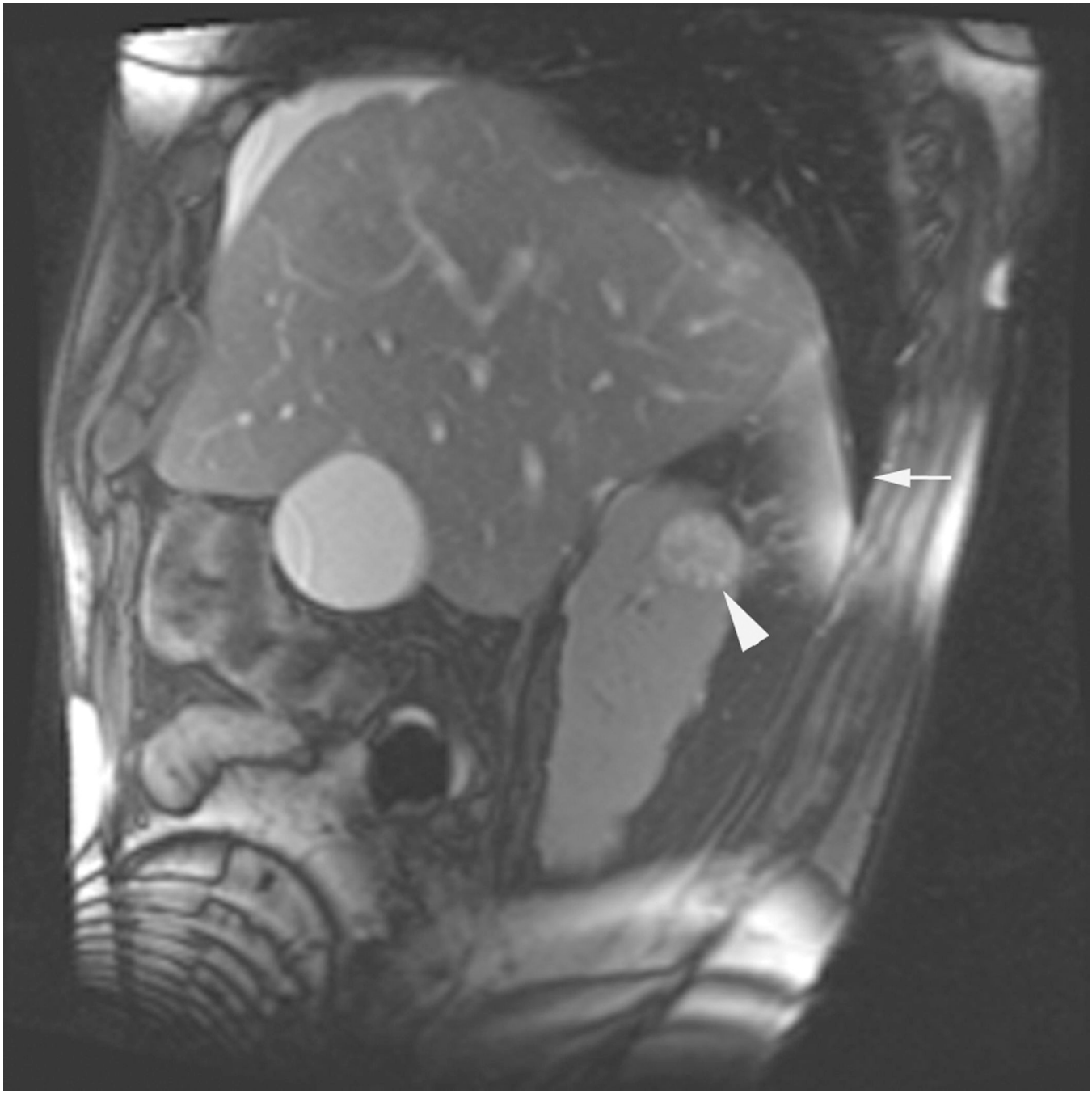

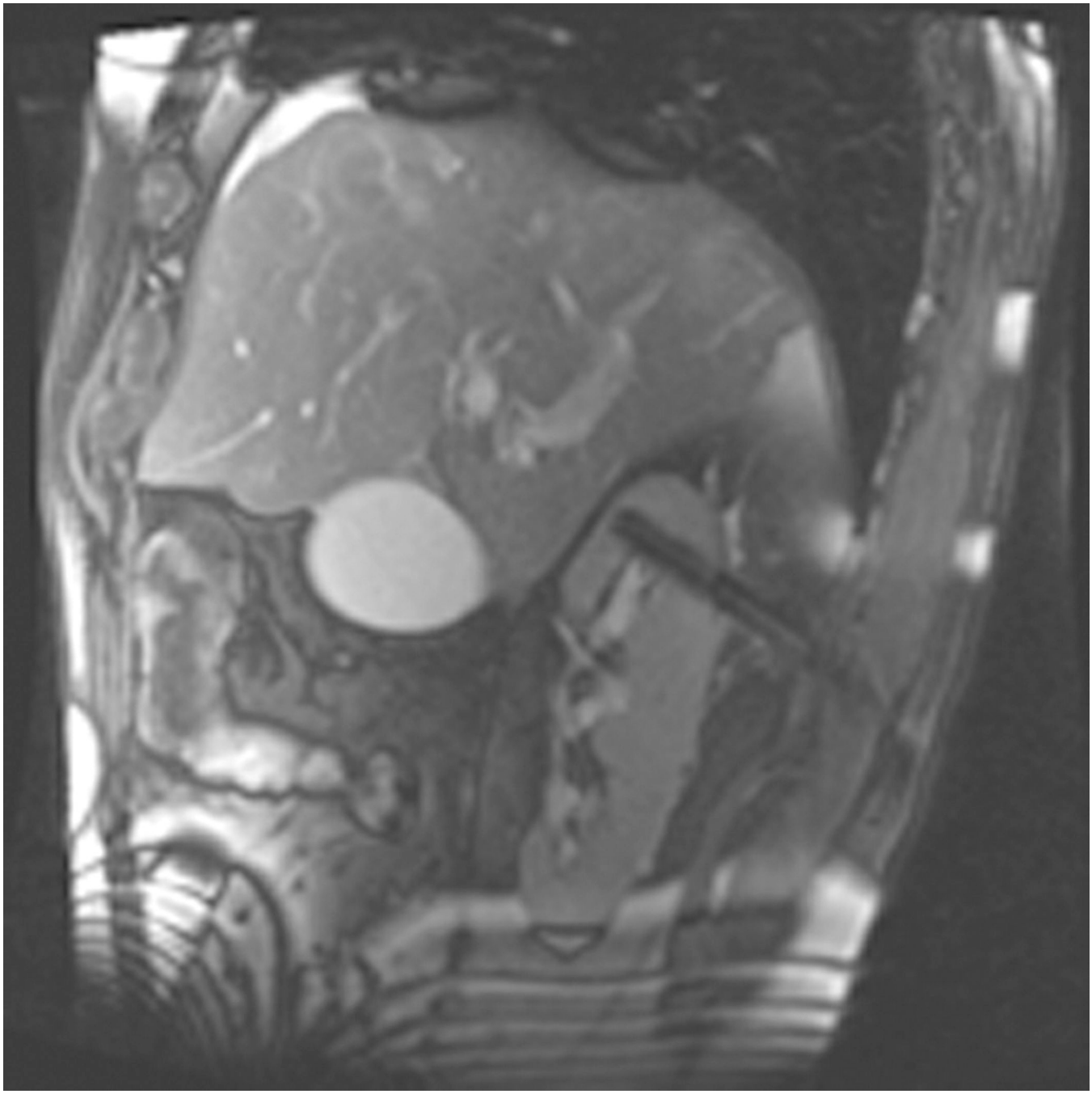

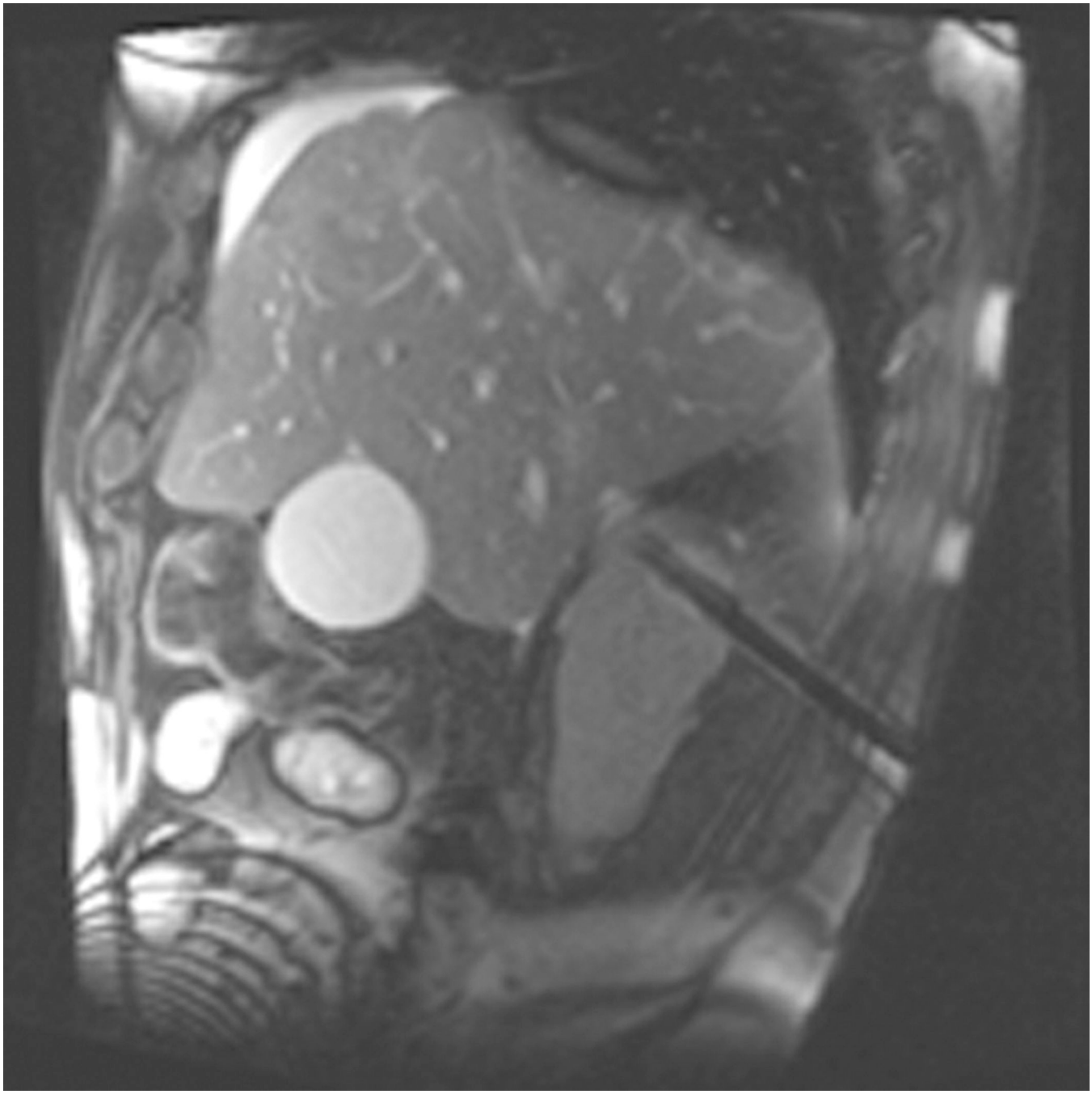

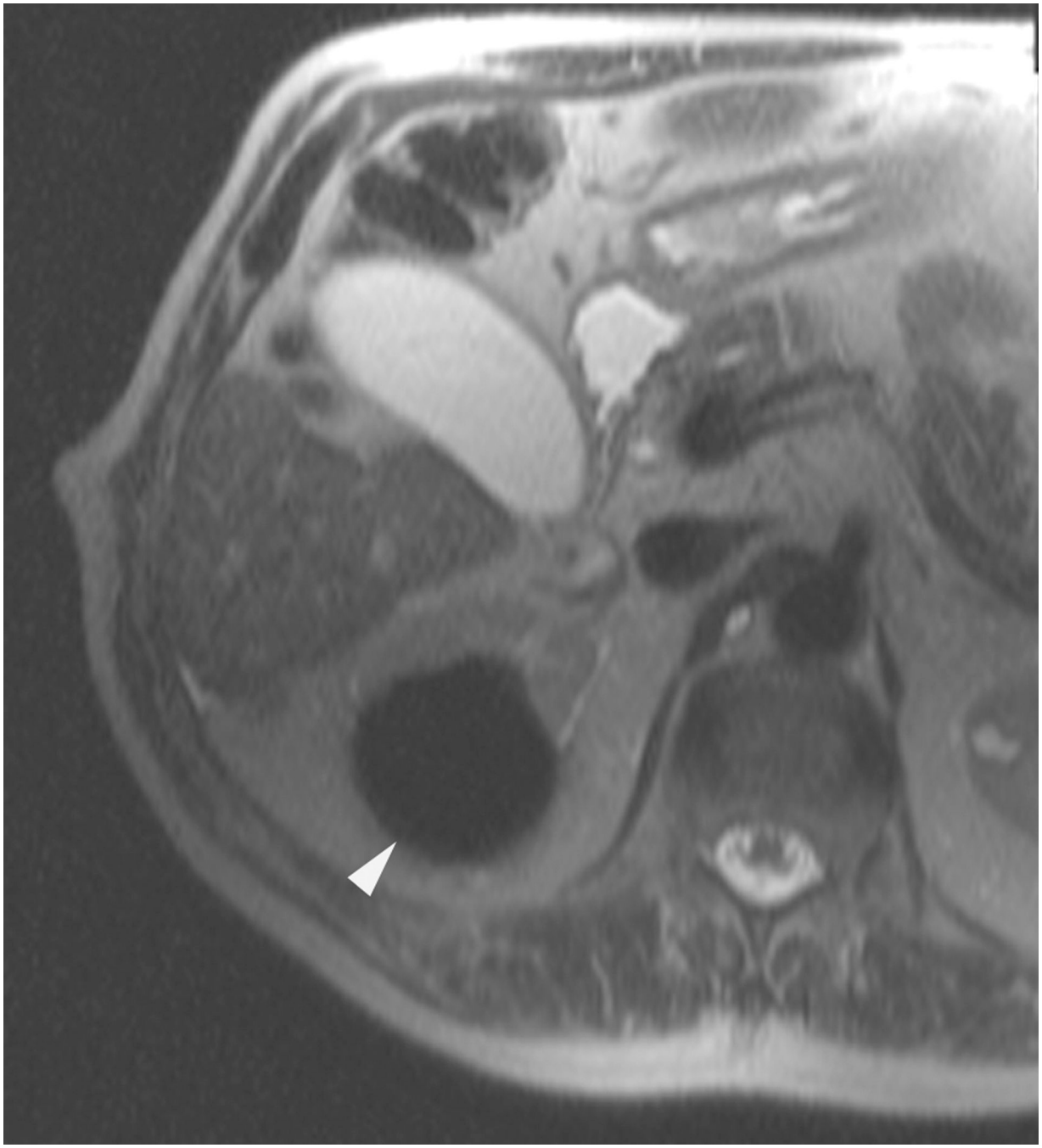

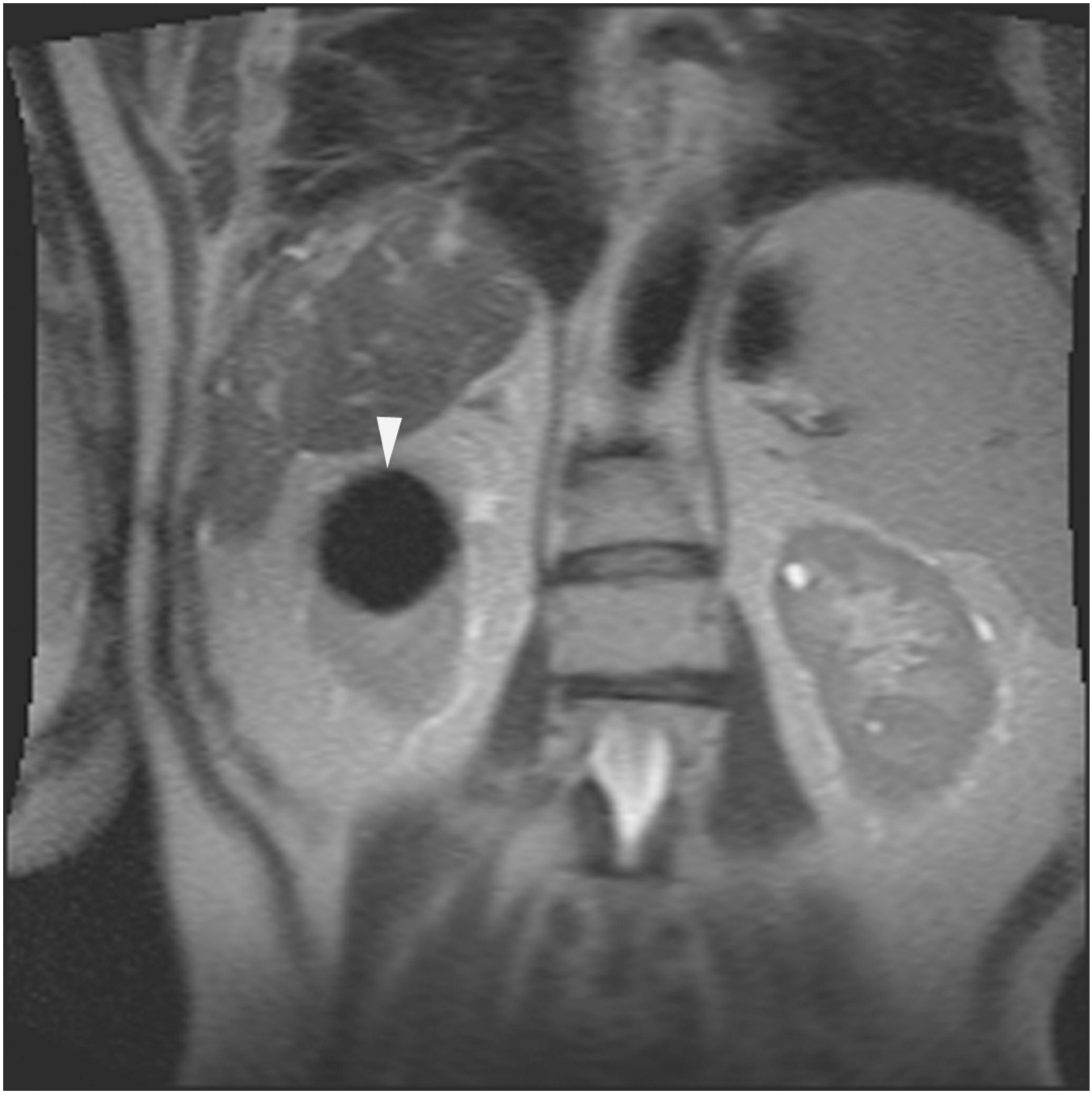

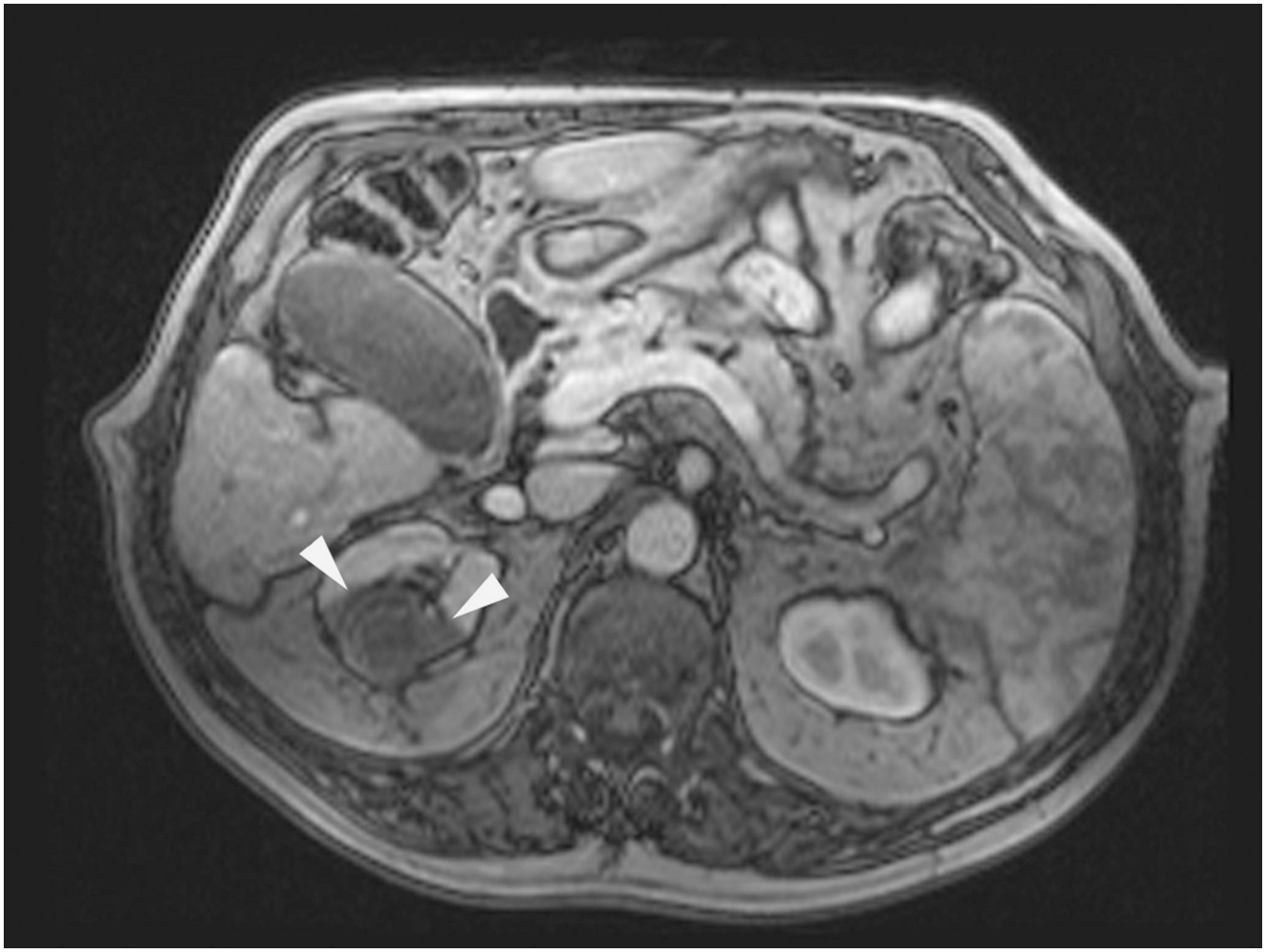

Figure 1.

A 70 year-old man with history of colon cancer underwent CT imaging for staging purposes. Axial CT image of the abdomen after intravenous administration of contrast (a) shows a 2.5 cm incidental mass (arrowheads) in the right kidney. He was referred for percutaneous biopsy. Non-contrast, axial CT image of the right kidney in prone position (b) shows intervening lung in the base of the right pleural cavity (arrow). The tumor (arrowhead) is isodense with normal kidney and is difficult to identify. Patient was placed in the right lateral decubitus position to decrease the right lung volume and was given iodinated contrast to better delineate the tumor margins for the biopsy (c). Pathology showed renal cell carcinoma, clear cell type, Fuhrman nuclear grade 2. Subsequently, he was referred for image guided ablation. Considering that the tumor was isodense to the kidney on CT images and the fact that intervening lung precluded placement of cryoprobes in an axial plane, a decision was made to perform the ablation under MRI guidance rather than CT. Sagittal T2-weighted image of the kidney (d) clearly demonstrates a hyperintense tumor (arrowhead) in the upper pole of the right kidney. Intervening lung parenchyma is identified posterior to the tumor (arrow). Using a sagittal plane of imaging, three cryoprobes were inserted into the tumor from an inferior approach to avoid puncturing the lung. Probes were placed under real-time MRI guidance in the medial (e), center (f), and lateral (g) border of the tumor. Axial (h), sagittal (i), and coronal (j) T2-weighted images of the kidney performed using a HASTE sequence show a hypointense ice ball (arrowheads) covering the entire tumor with

adequate margins. Post-treatment dynamic contrast-enhanced MRI (k) demonstrates perfusion deficit (arrowheads) within the expected area of damage based on the MRI monitoring feedback.

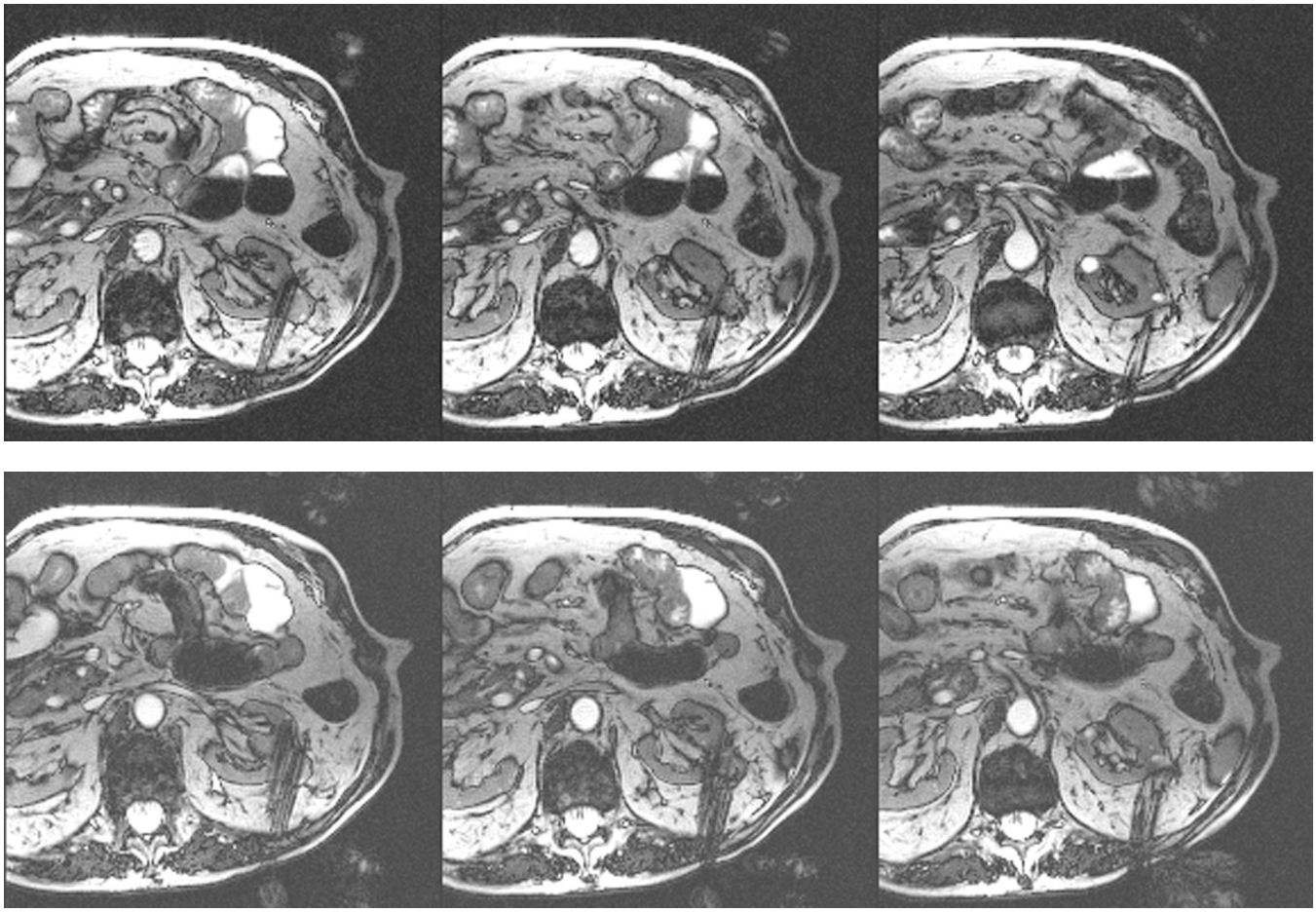

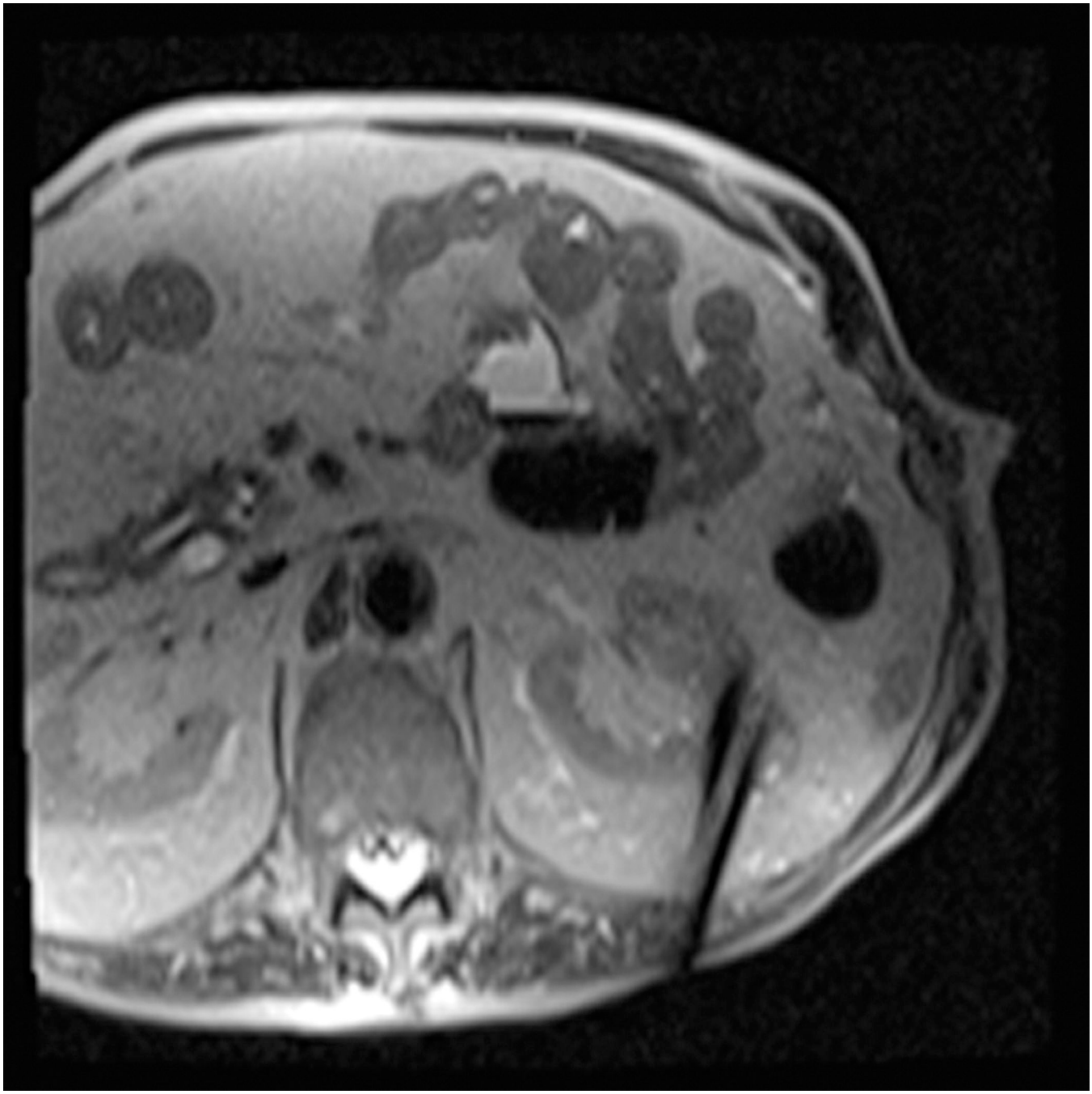

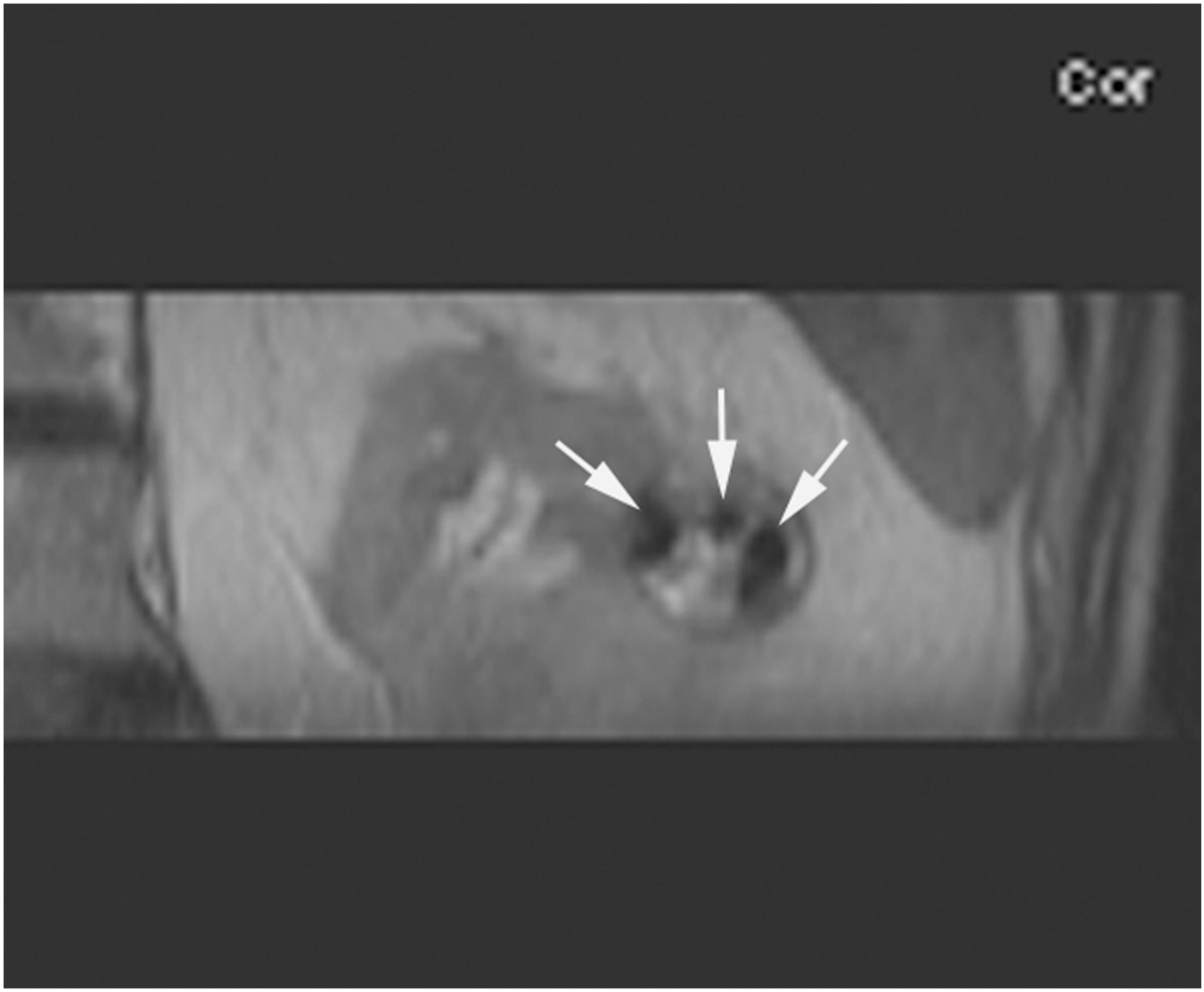

Figure 2.

An 80 year old man was found to have a 0.8 cm mass in the left kidney. He was initially managed by active surveillance. Repeat imaging showed enlargement of the tumor to 2.8 cm. Biopsy showed renal cell carcinoma, clear cell type, Fuhrman nuclear grade 2. He was referred for image-guided ablation. Axial T2-weighted (bSSFP) MRI of the abdomen in prone position (a) shows a hyperintense mass in the lateral aspect of the left kidney. The first cryoprobe was inserted into the medial border of the mass (b) under real-time MRI guidance (prtototype bSSFP sequence). Three parallel sequentially acquired images (4 mm thick with 1 mm gap) are displayed and updated at a rate of < 1 second per slice (b). The center image is the center slice, the image to the left is the inferior plane, and the image on the right is the superior plane. These three parallel images help monitor any deviation of the probe from its intended course. The operator can adjust the angle as needed and continue to insert the probe under real time MRI guidance. Another set of images (c) shows placement of the second probe in the lateral aspect of the tumor. Susceptibility induced signal losses degraded the quality of the bSSFP acquisition (c). Axial images were obtained using a HASTE sequence to better delineate the position of the probes (d). After insertion of the third probe under real-time guidance, a 3-D HASTE sequence was performed. Reconstructed coronal image (e)

shows the distribution of the probes within the tumor (arrows). Note that the scanner displays the image in the default radiological coordinates (ventral surface at top of image) despite the fact that the patient is placed in prone position.

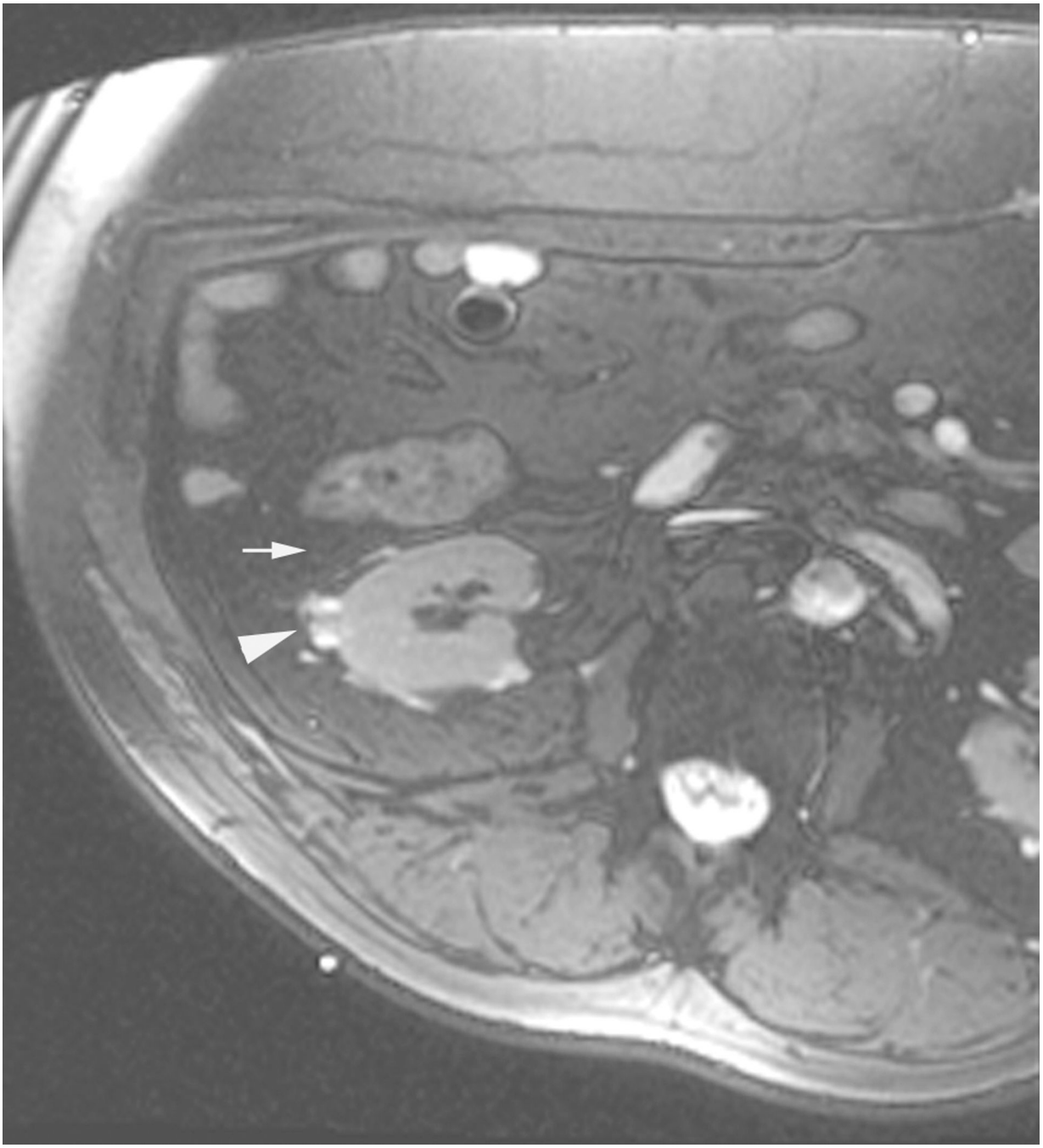

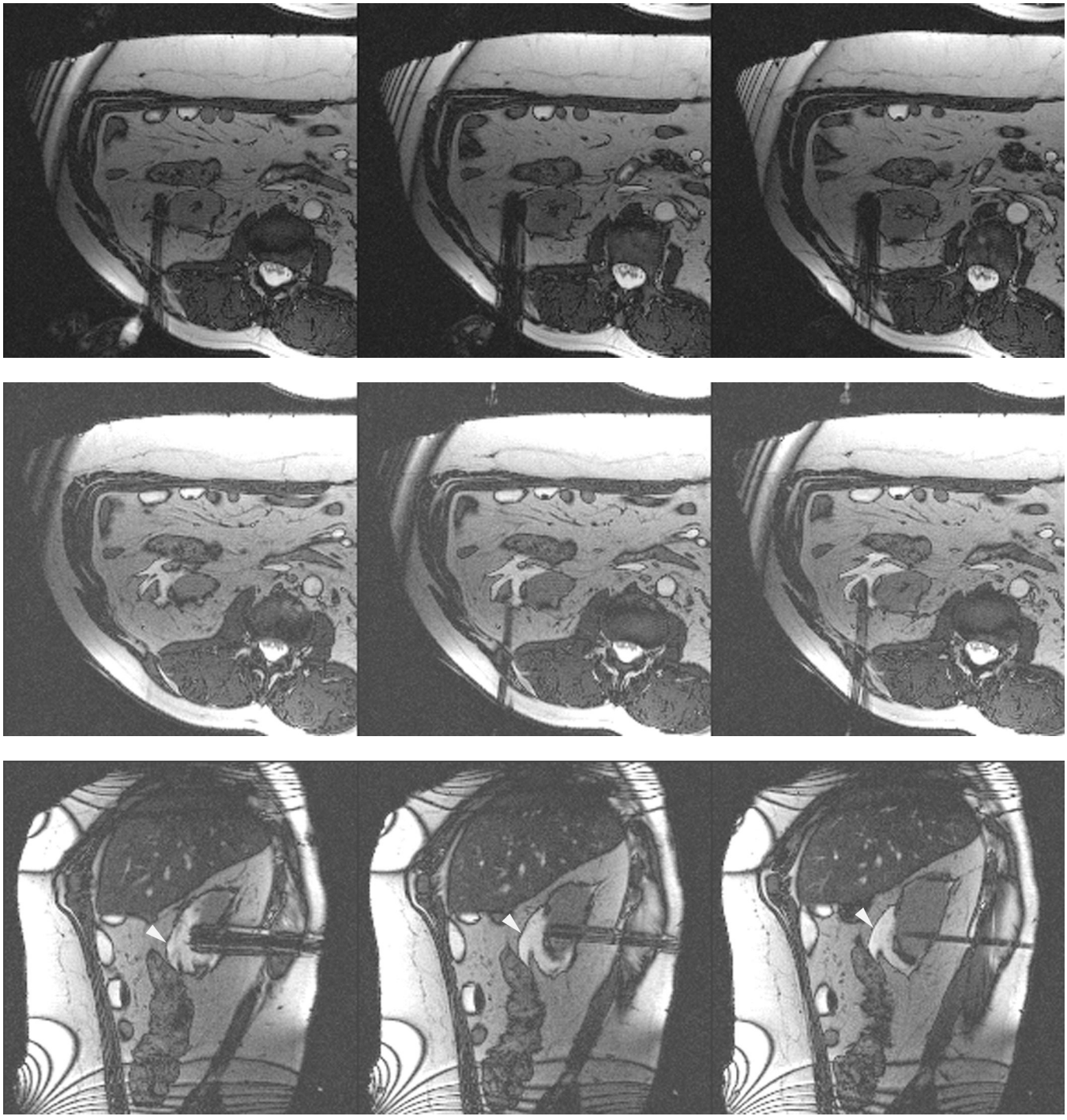

Figure 3.

Axial (a) and sagittal (b) T2-weighted (bSSFP) images of the right kidney show a hyperintense, exophytic mass (arrowheads). Biopsy showed renal cell carcinoma, clear cell type, Fuhrman nuclear grade 2. Adequate retroperitoneal fat (arrows) separated the tumor from the colon located anterior to the kidney. Once the cryoprobes were inserted into the tumor, real-time images (c) demonstrated close proximity of the colon to the cryoprobes. A 22 gauge needle was inserted under real-time MRI guidance in the perinephric space and 60 ml of saline was injected to separate the colon from the kidney. Axial (d) and sagittal (e) real-time images show successful hydrodissection with fluid (high intensity) widening the space between the kidney and the colon. Sagittal HASTE MR image of the kidney during

ablation shows the hypodense ice ball (f) separated from the colon by a layer of fluid, rendering the ablation safe.

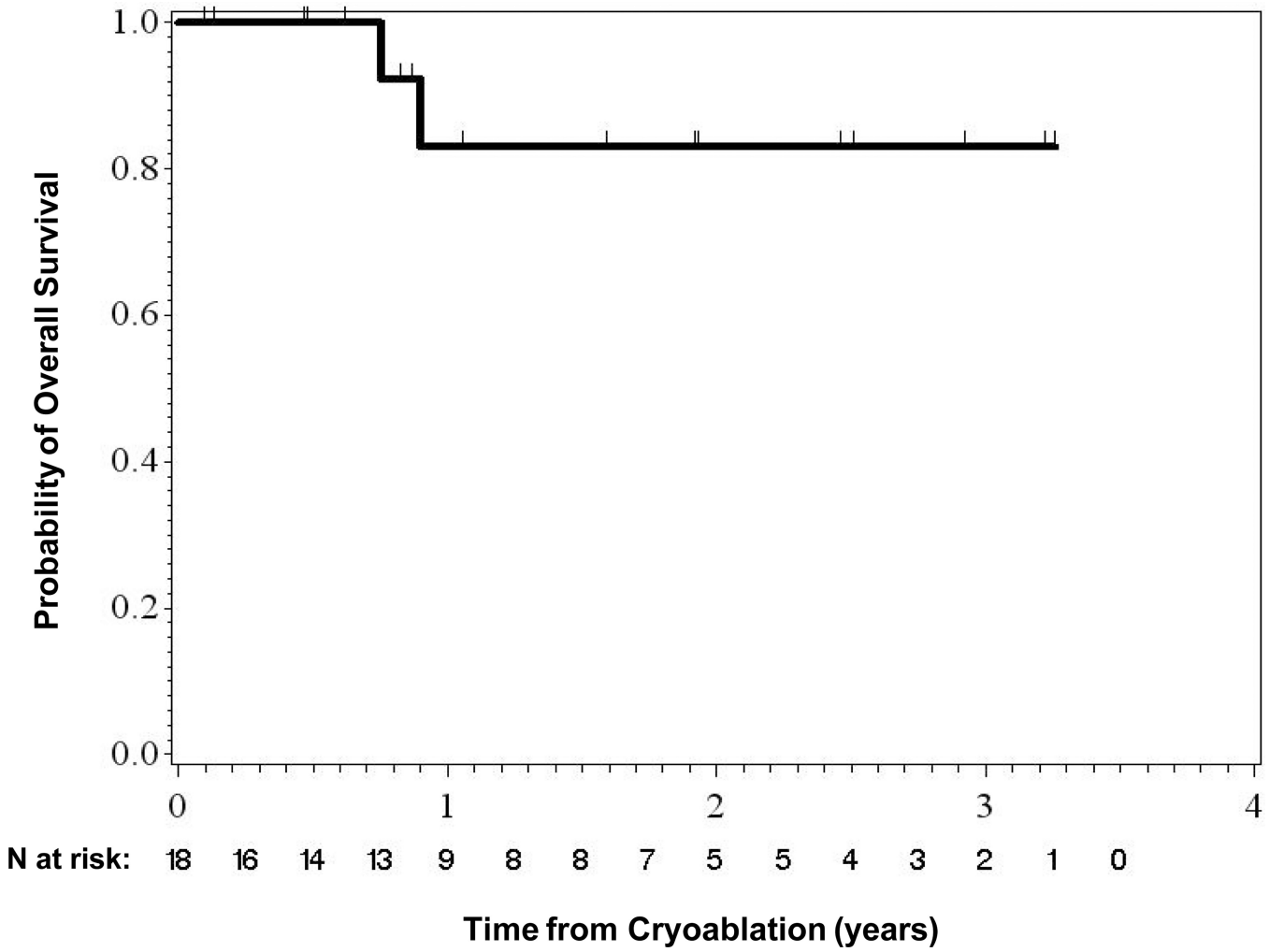

Figure 4.
Overall Survival

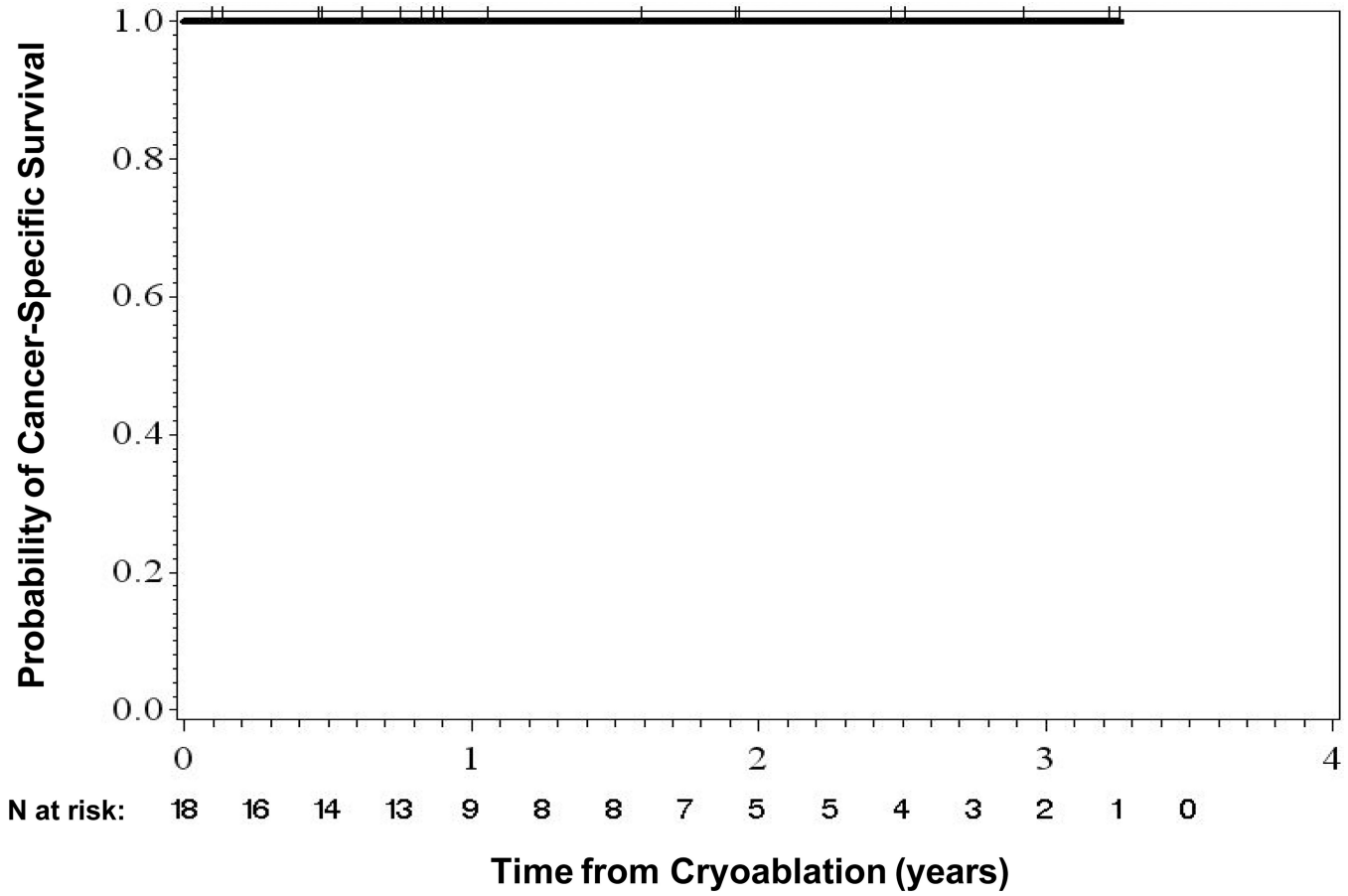

Figure 5.
Cancer-Specific Survival

Table 1

Specific parameters for the acquisitions

Acquisition	Planning	Targeting*	Target Verification		Monitoring	Verification
Sequence	**bSSFP (‘trueFISP’)**	**bSSFP (‘BEAT_IRTTT’)**	**bSSFP (‘trueFISP’)**	**HASTE**	**HASTE**	**3D FSPGR (‘VIBE’)**
TR (ms)	<4	<4	<4	2000	2000	6
TE (ms)	<3	<3	<3	83	83	2.8
Flip Angle	55–70	55–70	55–70	**	**	15
Matrix	256×192	192×192	256×192	192×192	192×192	256×134***
FOV (cm)	20–36	20–36	20–36	20–36	20–36	35×26
Slice/Skip (mm/mm)	5/0	4/1	5/0	“	“	5/2.5
BW (Hz/pix.)	500–800	500–800	500–800	400–500	400–500	250
Slices	15–25	3	15–25	“	“	52
Acq. Time (s)	< 1sec/img	<0.8 sec/img	<0.8 sec/img	2 sec/img	2 sec/img	<20 sec/acq

* Prototype interactive bSSFP pulse sequence, Siemens Corporate Research, sequence author: Li Pan

** Standard 90° excitation with 150° refocusing pulses

*** Parallel imaging acquisition and reconstruction (GRAPPA) with 75% phase field of view and 70% sampling in slice direction.

Table 2

Patient Characteristics

Measures	N=18
Age (years)	
Mean (SD)	66.6 (10.3)
Median	68.8
Range	40.7 – 81.5
Gender, n (%)	
Male	12 (66.7)
Female	6 (33.3)
BMI (kg/m^2)	
Mean (SD)	28.9 (5.6)
Median	28.9
Range	20.7 – 42.7
Size of tumor (cm)	
Mean (SD)	2.2 (0.7)
Median	2.0
Range	1.2 – 4.4
Side of Body, n (%)	
Right	9 (50.0)
Left	9 (50.0)

Abbreviation: SD = standard deviation.